

## The dependence of the ice-albedo feedback on atmospheric properties

P. von Paris<sup>1,2,3</sup>, F. Selsis<sup>1,2</sup>, D. Kitzmann<sup>4</sup>, H. Rauer<sup>3,4</sup>

<sup>1</sup> Univ. Bordeaux, LAB, UMR 5804, F-33270, Floirac, France

<sup>2</sup> CNRS, LAB, UMR 5804, F-33270, Floirac, France

<sup>3</sup> Institut für Planetenforschung, Deutsches Zentrum für Luft- und Raumfahrt,  
Rutherfordstr. 2, 12489 Berlin, Germany

<sup>4</sup> Zentrum für Astronomie und Astrophysik, Technische Universität Berlin,  
Hardenbergstr. 36, 10623 Berlin, Germany

Corresponding author:

Philip von Paris

Email: philip.vonparis@dlr.de

Tel.: +49 (0) 30- 67055 7939

## **Abstract**

The ice-albedo feedback is a potentially important de-stabilizing effect for the climate of terrestrial planets. It is based on the positive feedback between decreasing surface temperatures, an increase of snow and ice cover and an associated increase in planetary albedo, which then further decreases surface temperature. A recent study shows that for M stars, the strength of the ice-albedo feedback is reduced due to the strong spectral dependence of stellar radiation and snow/ice albedos, i.e. M stars primarily emit in the near-IR, where the snow and ice albedo is low, and less in the visible where the snow/ice albedo is high.

This study investigates the influence of the atmosphere (in terms of surface pressure and atmospheric composition) for this feedback, since an atmosphere was neglected in previous studies. A plane-parallel radiative transfer model is used for the calculation of planetary albedos. We varied CO<sub>2</sub> partial pressures as well as the H<sub>2</sub>O, CH<sub>4</sub>, and O<sub>3</sub> content in the atmosphere for planets orbiting Sun-like and M-type stars.

Results suggest that for planets around M stars, the ice-albedo effect is significantly reduced, compared to planets around Sun-like stars. Including the effects of an atmosphere further suppresses the sensitivity to the ice-albedo effect. Atmospheric key properties such as surface pressure, but also the abundance of radiative trace gases can considerably change the strength of the ice-albedo feedback. For dense CO<sub>2</sub> atmospheres of the order of a few to tens of bar, atmospheric rather than surface properties begin to dominate the planetary radiation budget. At high CO<sub>2</sub> pressures, the ice-albedo feedback is strongly reduced for planets around M stars. The presence of trace amounts of H<sub>2</sub>O and CH<sub>4</sub> in the atmosphere also weakens

the ice-albedo effect for both stellar types considered. For planets around Sun-like stars, O<sub>3</sub> could also lead to a very strong decrease of the ice-albedo feedback at high CO<sub>2</sub> pressures.

# 1 Introduction

The ice-albedo feedback is a very important positive feedback for the Earth's climate. In simple words, it describes the possible runaway cooling of the planetary surface. Decreasing surface temperature leads to an increase of snow and ice cover, which increases the surface albedo. Hence, more incoming stellar radiation is reflected back to space, which in turn decreases surface temperature.

A recent work by Joshi and Haberle (2012) connected this ice-albedo feedback to exoplanets and the habitable zone (HZ). The HZ is defined as the region around a star where a planet with a suitable atmosphere could have liquid water on the surface, hence the potential for life as we know it (Kasting et al. 1993). Calculations presented by Joshi and Haberle (2012) showed that the planetary albedos for planets orbiting M stars are much lower than for planets orbiting Sun-like stars because of the strong spectral dependence of both ice and snow albedo and the stellar spectrum. Hence, the ice-albedo feedback is much less important for planets orbiting M stars. Based on these results, Joshi and Haberle (2012) stated that the outer boundary of the HZ is more extended around M stars than around G stars since planetary albedos are much lower.

However, the ice-albedo feedback is not the key factor when determining the extent of the outer boundary of the HZ. It is usually assumed that geochemical cycles such as the carbonate-silicate cycle (e.g., Walker et al. 1981; Abbot et al. 2012) will stabilize the climate (e.g., Kasting et al. 1993; Selsis et al. 2007). The outer boundary of the HZ is then determined by the interplay between an increase of planetary albedo with increasing CO<sub>2</sub> and the atmospheric greenhouse effect provided by CO<sub>2</sub> (Kasting et al. 1993). A higher planetary albedo does not neces-

sarily imply lower surface temperatures, as has been shown by, e.g., McKay et al. (1989), or Mischna et al. (2000). Still, at one point, an increase in planetary albedo will lead to cooler surface temperatures, an effect known for CO<sub>2</sub> as the maximum greenhouse effect (Kasting et al. 1993). Furthermore, atmospheres towards the outer edge of the HZ are assumed to be very dense (of the order of several bars of CO<sub>2</sub>, Kasting et al. 1993), implying that the influence of surface albedo on the planetary energy budget is probably rather small (see, e.g., Wordsworth et al. 2011 for 3D investigations of the outer HZ). Therefore, conclusions on habitability and the extent of the HZ cannot be easily drawn from the investigation of the ice-albedo feedback.

Nevertheless, the ice-albedo feedback is still an important process for the atmospheric and climate evolution of the Earth. It is generally accepted that Earth encountered several global glaciation episodes (the so-called snowball Earth, e.g., Kirschvink 1992, Hoffman et al. 1998, Hyde et al. 2000, Kasting and Ono 2006) and, more recently, ice ages with widespread glaciations down to mid-latitudes (e.g., Tarasov and Peltier 1997). Some of these snowball episodes coincide with major events in the evolution of the biosphere, such as the advent of atmospheric O<sub>2</sub> (Kasting and Howard 2006; Goldblatt et al. 2006) and multicellular organisms (Hyde et al. 2000). Rapid, perhaps geologically or biologically induced, changes in atmospheric composition might have been responsible for triggering these glaciations (e.g., Pavlov et al. 2003).

Therefore, it is of interest for astrobiology and a comprehensive theory of atmospheric evolution to investigate whether planets orbiting other central stars might also be subject to such feedbacks. The work by Joshi and Haberle (2012) calculated planetary albedos based on surface albedos and did not take explicitly

the atmosphere into account. However, atmospheric properties such as surface pressure or atmospheric composition have a potentially large influence on the planetary albedo, hence the ice-albedo feedback. In this work, we present similar calculations as in Joshi and Haberle (2012), but with a plane-parallel radiative transfer model which incorporates the radiative effects of an atmosphere. The model is used to calculate planetary albedos of prescribed atmospheric scenarios when varying atmospheric properties (such as atmospheric composition and surface pressure). In a complementary approach, Shields et al. (2013) used a combination of 2D and 3D models to assess the development of ice and snow cover on planets orbiting M, G, and F stars upon decreasing stellar insolation. However, the considered planetary atmospheres were Earth-like in terms of surface pressure and composition. With a 1D radiative transfer model, Shields et al. (2013) also calculated planetary albedos as a function of CO<sub>2</sub> partial pressure, however without considering additional trace species, such as water, ozone, or methane.

The paper is organized as follows: Sect. 2 presents the model and scenarios, Sect. 3 the results and Sect. 4 a discussion of additional aspects. We summarize the results and conclude with Sect. 5.

## **2 Methods**

### **2.1 Radiative transfer**

We used a plane-parallel radiative transfer model to obtain planetary albedos of a wide range of prescribed, fixed atmospheric scenarios. The radiative fluxes important for the planetary albedo (i.e., stellar radiation) are calculated for a spec-

tral range of 0.237-4.545  $\mu\text{m}$ , divided into 38 spectral intervals. Scattering is treated based on a  $\delta$ -Eddington-2-stream algorithm summarized by Toon et al. (1989). The frequency integration is performed using correlated-k coefficients in up to 4-term exponential sums (Wiscombe and Evans 1977). Gaseous opacities are taken from Pavlov et al. (2000) and Karkoschka (1994). Rayleigh scattering is incorporated using approximations presented by von Paris et al. (2010), Vardavas and Carver (1984), and Allen (1973).

The pressure grid in the model atmospheres is determined from the surface pressure  $p_{\text{surf}}$  up to a pressure of  $6.6 \times 10^{-5}$  bar at the model lid, divided into 52 model layers, approximately spaced equidistantly in log (pressure),

## 2.2 Model procedure

The planetary albedo  $A_p$  is calculated as a Bond albedo in the model, i.e.

$$A_p = \frac{F_u}{F_*} = \frac{\int_0^\infty A_{p,\lambda} \cdot F_{*,\lambda} d\lambda}{\int_0^\infty F_{*,\lambda} d\lambda} \quad (1)$$

where  $F_u$  is the spectrally integrated upwelling shortwave flux at the top of the atmosphere,  $F_*$  the total stellar insolation,  $A_{p,\lambda}$  the spectral albedo and  $F_{*,\lambda}$  the spectral stellar insolation. As can be seen easily from this formulation, the planetary albedo of a given atmosphere is independent of orbital distance.  $F_{*,\lambda}$  was approximated by stellar spectra for the Sun (as a G-star proxy) and AD Leo (representing an M-type star, with 0.41 solar radii, 0.4-0.5 solar masses and an effective temperature of  $\approx 3,400$  K, see e.g. Leggett et al. 1996, Segura et al. 2005). Spectra were taken from Kitzmann et al. (2010) and are shown in Fig. 1. The total stellar insolation is scaled to modern-day Earth insolation (i.e.,  $F_* = 1,366 \text{ Wm}^{-2}$ ).

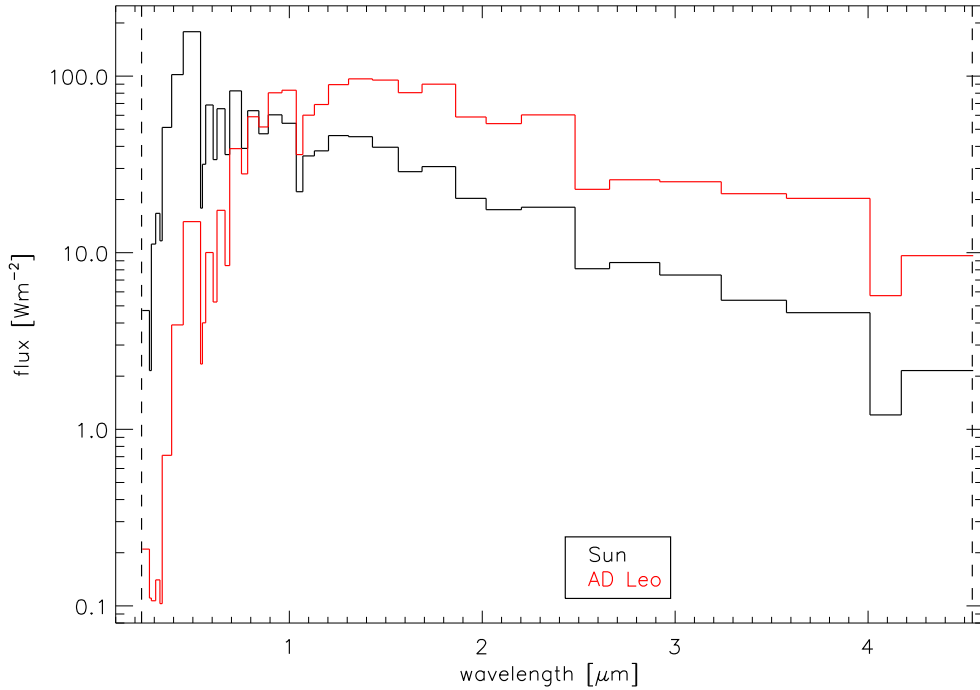


Figure 1: Stellar spectra of the Sun and AD Leo as used in this work, normalized to equal modern-day Earth insolation. Vertical dashed lines indicate the spectral boundaries of the radiative transfer scheme ( $0.237\text{-}4.545\ \mu\text{m}$ , see Sect. 2.1).

To investigate the influence of different atmospheric and surface properties on planetary albedo, we prescribed atmospheric composition, the surface pressure and the temperature profile for our calculations. Unless otherwise specified, the temperature profile was fixed at the modern-Earth profile  $T_m(z)$  ( $z$  altitude), taken from Grenfell et al. (2011). The stellar zenith angle was fixed at  $60^\circ$  to simulate globally averaged conditions.



### 2.3 Parameter variations

We used two different types of surface albedo parameterizations. The first parametrization employed the wavelength-dependent surface albedos  $A_S$  of ice and snow, as shown in Fig. 2. We took spectral albedo data presented in Joshi and Haberle (2012), which were originally obtained from measurements in Antarctica (Brandt et al. 2005, Hudson et al. 2006). Note that the albedo remains constant at wavelengths  $\gtrsim 1.5 \mu\text{m}$  (for ice, Brandt et al. 2005) and  $\gtrsim 2.4 \mu\text{m}$  (for snow, Hudson et al. 2006) since respective measurements were restricted to these spectral ranges. The second parametrization used a constant (wavelength-independent) surface albedo (values of 0.1, 0.2, 0.7 and 0.9, with 0.1 being close to present Earth’s mean surface albedo, Rossow and Schiffer 1999).

The most important parameter for determining the location of the outer edge of the habitable zone is the  $\text{CO}_2$  partial pressure. We performed calculations for 22  $\text{CO}_2$  partial pressures ranging between 0.1 and 30 bar.

Since  $\text{H}_2\text{O}$  has very strong visible and near-IR absorption bands, even low concentrations could have an important impact on calculated albedos. To investigate this further, we performed simulations with the ice and snow surface albedos and atmospheres containing varying amounts of  $\text{H}_2\text{O}$ .  $\text{H}_2\text{O}$  concentrations  $c_{\text{H}_2\text{O}}$  as a function of altitude  $z$  were set to follow the temperature-dependent saturation vapor pressure  $p_{\text{vap,H}_2\text{O}}(T)$ , i.e. model atmospheres were assumed to be fully saturated:

$$c_{\text{H}_2\text{O}}(z) = \frac{p_{\text{vap,H}_2\text{O}}(T(z))}{p(z)} \quad (2)$$

Atmospheric temperatures  $T(z)$  were set to the modern-Earth profile (i.e.,  $T(z) =$

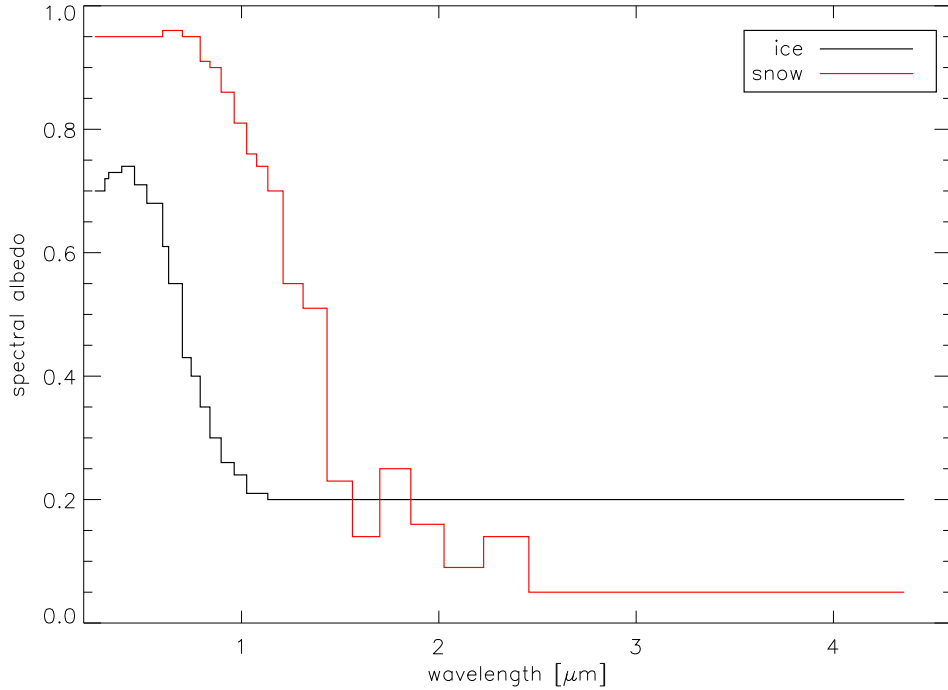


Figure 2: Snow and ice spectral albedo. Taken from Joshi and Haberle (2012), their Fig. 1, data from Brandt et al. (2005) and Hudson et al. (2006).

$T_m(z)$ , see Sect. 2.2) and to a colder profile with  $T(z) = T_m(z) - 15$  (corresponding to a surface temperature of 273 K). The colder temperature profile resulted in an approximate decrease in  $H_2O$  column amount of about a factor of 5-6.

$CH_4$  can build up in the atmosphere if strong surface fluxes exist, as postulated for, say, early Earth (e.g., Pavlov et al. 2003). Planets around M stars favor a build-up of  $CH_4$  because of the weak stellar UV radiation field and the related HOx chemistry (less OH means more  $CH_4$ , see e.g. Segura et al. 2005 or Grenfell et al. 2007).  $CH_4$  could have an important effect on the planetary albedo because of strong near-IR absorption bands. To investigate this, we performed calculations with  $CH_4$  concentrations set to an isoprofile with concentrations of  $10^{-6}$ ,  $10^{-4}$  and

Table 1: Parameters for the model calculations performed (vmr volume mixing ratio, PAP present atmospheric profile,  $w$ : warm temperature profile  $T_m$ ,  $c$ : cold temperature profile  $T_m - 15$ , see Eq. 2).

Scenario	$A_S$	$p_{\text{CO}_2}$ [bar]	$\text{H}_2\text{O}$	$\text{CH}_4$ vmr	$\text{O}_3$ [PAP]
1	snow, ice (Fig. 2)	0.1, 0.2,...,1, 2,...,10,...,30	0	0	0
2	0.1, 0.2, 0.7, 0.9	0.1, 0.2,...,1, 2,...,10,...,30	0	0	0
3	snow, ice (Fig. 2)	0.1, 0.2,...,1, 2,...,10,...,30	$w, c$	0	0
4	snow, ice (Fig. 2)	0.1, 0.2,...,1, 2,...,10,...,30	0	$10^{-6}, 10^{-4}, 10^{-3}$	0
5	snow, ice (Fig. 2)	0.1, 0.2,...,1, 2,...,10,...,30	0	0	1,10

$10^{-3}$ , respectively (again, with the ice and snow surface albedos).

$\text{O}_3$  can build up abiotically in  $\text{CO}_2$ -rich or strongly UV-irradiated atmospheres to quite large concentrations (e.g., Selsis et al. 2002, Segura et al. 2007, Domagal-Goldman and Meadows 2010) and could furthermore be the by-product of an oxygen-producing biosphere. It features strong absorption bands in the UV and visible part of the spectrum where Rayleigh scattering is strongest. Therefore, we performed sensitivity studies where we introduced an artificial ozone profile in the model atmospheres (1x and 10x modern Earth’s concentrations following a mean Earth profile from Grenfell et al. 2011, with the ice and snow surface albedos). We note that 10x modern Earth levels most likely represent upper limits for the  $\text{O}_3$  profile. However since we aim at performing sensitivity studies only, we take this case as an end-member case.

All the simulations were done for an AD Leo and a Sun spectrum (see Fig. 1). Table 1 summarizes the scenarios.

Note that we did not include  $\text{N}_2$  in our model atmospheres, despite the fact that it is present in substantial amounts in all terrestrial atmospheres of the solar system (i.e., Venus, Earth, Mars, Titan). The reason is that  $\text{N}_2$  does not feature absorption bands or lines in the visible and near-IR which are strong enough to

affect the albedo and its Rayleigh scattering coefficient is nearly a factor of three smaller than for CO<sub>2</sub> (Vardavas and Carver 1984).

## 3 Results

### 3.1 Atmospheric flux profiles

Figure 3 shows the downwards and upwards flux profiles in the visible/near-IR spectral domain as a function of pressure for the 0.1 bar and the 20 bar ice case of scenario 1 from Table 1. It is clearly seen that in the case of a 0.1 bar CO<sub>2</sub> atmosphere, the influence of the atmosphere on these radiative fluxes, hence the influence on the planetary albedo, is rather small. The profiles all remain approximately constant throughout the entire atmosphere in this case. In contrast to that, in the 20 bar scenario, the atmospheric influence is very strong.

For the planet around the Sun, the incoming stellar flux is roughly reduced by a factor of 2 (black line, 340 Wm<sup>-2</sup> incoming flux at the top of the atmosphere, ~ 160 Wm<sup>-2</sup> reaching the surface). Most of this radiation is reflected back to space due to very efficient Rayleigh scattering (red line). The surface albedo contributes around 70 Wm<sup>-2</sup> to the upwards flux at the top of the atmosphere, while the Rayleigh scattering component amounts to 120 Wm<sup>-2</sup>.

For the planet around the M-dwarf AD Leo, the influence of the atmosphere in the 20 bar scenario is also very prominent. However, in this case it is primarily due to the absorption of near-IR radiation by CO<sub>2</sub>. The surface and the Rayleigh scattering both contribute with about 50 % to the overall outgoing flux, but in absolute terms, the Rayleigh scattering component is reduced to about 35 Wm<sup>-2</sup>

(i.e., almost a factor of 4 compared to the Sun). The stellar flux reaching the surface is reduced from  $340 \text{ Wm}^{-2}$  to less than  $150 \text{ Wm}^{-2}$ , which is only slightly less than for the planet around the Sun. Comparing the Rayleigh scattering component with the reduction in downwards flux, one finds that approximately  $150 \text{ Wm}^{-2}$  are absorbed in the atmosphere.

It is noteworthy that although the planetary atmosphere has a huge impact on the flux profiles, in the case of the planet around AD Leo the planetary albedo does not change that much. In the 0.1 bar and the 20 bar scenario, both top-of-atmosphere outgoing flux values are nearly identical.

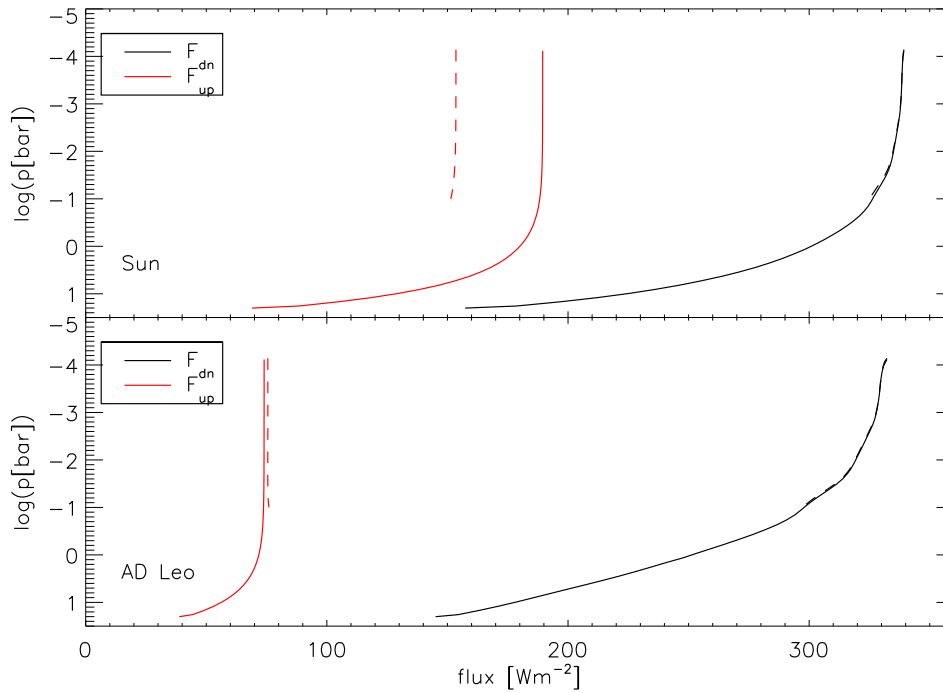


Figure 3: Net upward ( $F_{\text{up}}$ ) and downward ( $F_{\text{dn}}$ ) fluxes in the visible/near-IR for ice surface albedo (scenario 1 from Table 1). Pure  $\text{CO}_2$  atmospheres (20 bar plain lines, 0.1 bar dashed lines).

### 3.2 Planetary spectral albedo

Figure 4 shows the spectral albedos for three different values of the  $\text{CO}_2$  pressure of scenario 1 from Table 1. It is clearly seen that an increase of  $\text{CO}_2$  increases the spectral albedo in the visible (due to Rayleigh scattering) and decreases the spectral albedo in the near-IR (due to enhanced absorption). In general, the behavior of the spectral albedo follows the snow and ice spectral albedo in Fig. 2, i.e. a high spectral albedo in the visible and a rather low spectral albedo in the near-IR.

An important difference between ice and snow scenarios occurs near  $1\ \mu\text{m}$  where the calculated albedos differ by a factor of about 3. This spectral region is important since a rather large part of stellar radiation is emitted there.

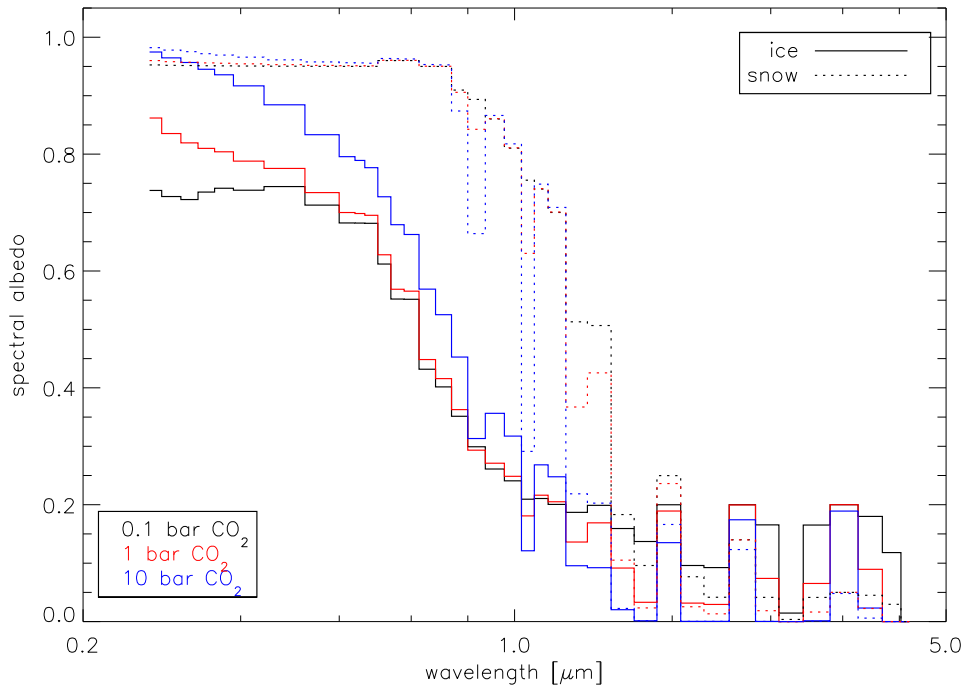


Figure 4: Spectral albedos for different values of  $\text{CO}_2$  pressure and ice and snow surface albedos. Pure  $\text{CO}_2$  atmospheres.

Note that for the visible part of the spectrum, where Rayleigh scattering is important, an increase of CO<sub>2</sub> from 0.1 bar to 10 bar does not significantly affect the spectral albedos for the snow surface case. In contrast, for the ice surface case, the effect is clearly distinguished. This is due to the very high visible albedo of snow (~0.9) in this spectral range, hence the surface reflection dominates the spectral albedo in the visible, independent of atmospheric conditions. The calculated values of the spectral albedos correspond well to values presented by Shields et al. (2013).

### **3.3 Planetary albedo**

Figure 5 shows the planetary Bond albedos of scenarios 1 and 2 from Table 1. The calculated values of planetary albedo with a very tenuous CO<sub>2</sub> atmosphere (0.1 bar) approximately confirm the values of Joshi and Haberle (2012) which were done without taking into account atmospheric effects (their Figure 2).

It is clearly seen that the central star type has a large effect on the planetary albedo. At high CO<sub>2</sub> partial pressures, planetary albedos for the planet around the Sun are 2-3 times higher than for the planet orbiting around AD Leo. This is of course due to the different spectral distribution of stellar energy (see Fig. 1). In terms of energy-equivalent orbital distance, this implies that planets around M-stars could be 10-20 % farther away from their central star and still receive the same net stellar energy input into the atmosphere. This fact is the basis for the claim of Joshi and Haberle (2012) that the HZ around M-stars is widened with respect to the HZ around G-stars.

As expected, planetary albedos are higher for snow surface albedo than for

ice surface albedo. However, with increasing  $\text{CO}_2$  partial pressure, the difference becomes noticeably smaller. For very dense, almost entirely optically thick atmospheres, planetary albedos will converge to a value independent of surface albedo.

Interestingly, the amount of  $\text{CO}_2$  has a rather weak effect on the planetary albedo when using ice and snow albedos. This was already implied in Figs. 3 and 4. The behavior of the atmospheric spectral albedo is similar to the spectral albedo of ice and snow (see Fig. 2). As before in Sect. 3.2, calculated values of Bond albedos correspond well to values in Shields et al. (2013).

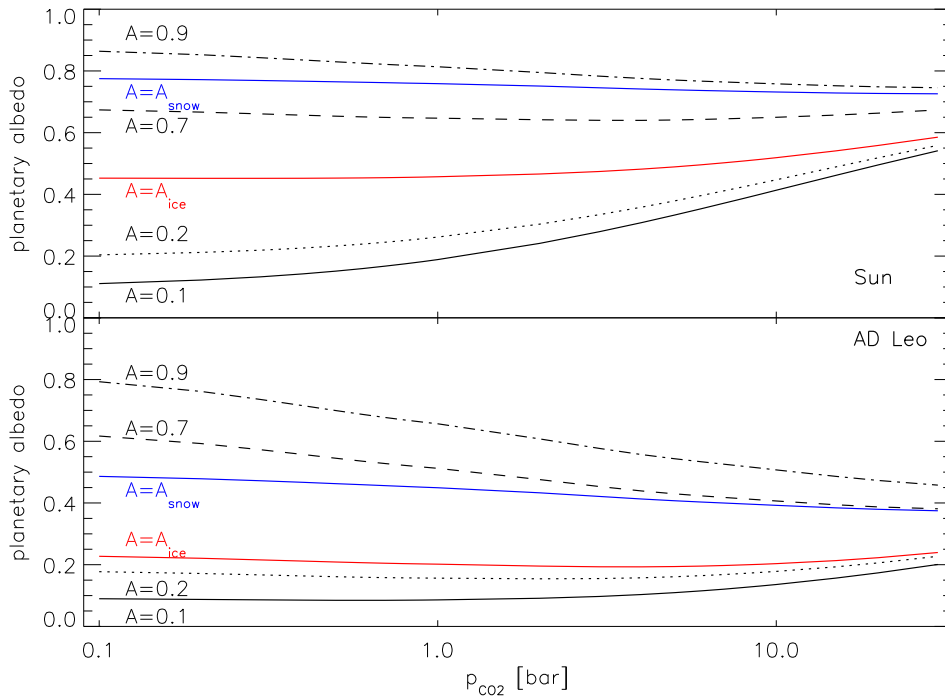


Figure 5: Planetary albedo as a function of  $\text{CO}_2$  pressure for scenarios 1 and 2 of Table 1. Pure  $\text{CO}_2$  atmospheres.

However, for a wavelength-independent surface albedo values, the effect of  $\text{CO}_2$  on planetary albedo is much stronger, especially for low (Sun) or high (AD



Leo) values of surface albedo. This is explained as follows. Scattering alone can only increase the albedo. Thus, in the case of a Sun-like irradiation, for which scattering-only is a fair approximation, the planetary albedo increases with pressure. Therefore, for a given range of pressure, the increase is more significant for low surface albedos. Absorption alone can only decrease the albedo. Thus, for AD Leo-like irradiation, for which absorption-only is a fair approximation, the planetary albedo decreases with pressure. The effect is more significant if the surface albedo is high. From Fig. 5 it is clear that the scattering-alone and absorption-alone approximations are not perfect. For the Sun and high surface albedos, Fig. 5 shows a slight decrease of planetary albedo when surface pressure increases which is due to CO<sub>2</sub> absorption in the near IR. For AD Leo and low surface albedos, the planetary albedo increases with pressure due to the scattering that becomes more significant.

### **Effect of atmospheric composition**

Fig. 6 shows the effect of increasing H<sub>2</sub>O concentrations on the calculated albedo. It is clearly seen that this decreases the planetary albedo. The effect is somewhat stronger for AD Leo than for the Sun. For example, for the ice surface albedo at 1 bar of CO<sub>2</sub>, when using the modern-day temperature profile and corresponding H<sub>2</sub>O profile (see Eq. 2), the planetary albedo decreases from 0.2 to 0.13 for AD Leo, but only from 0.45 to 0.40 for the Sun. This shows that even small amounts of water can enhance the effect of the stellar type on planetary albedo.

Fig. 7 shows the effect of increasing CH<sub>4</sub> concentration on the calculated albedo. Again, the effect is much stronger for AD Leo than for the Sun.

Fig. 8 shows the effect of increasing O<sub>3</sub> concentration on the calculated albedo.

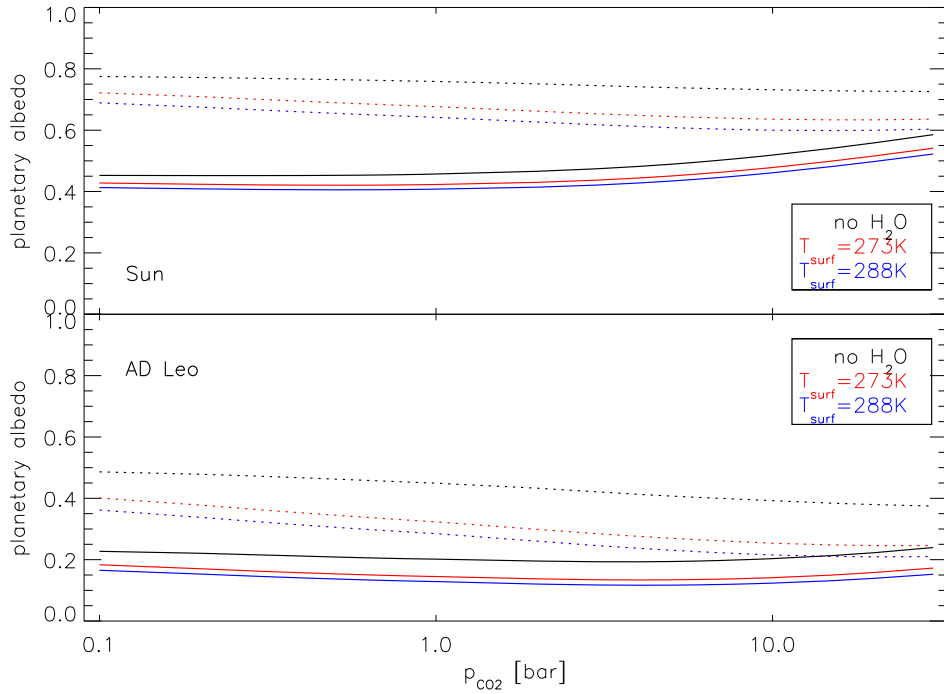


Figure 6: Planetary albedo as a function of CO<sub>2</sub> pressure for snow and ice surface albedos. Influence of H<sub>2</sub>O content. Plain lines for ice surface albedo, dotted lines for snow surface albedo.

It has a large impact for the Sun, but its effect is almost negligible for AD Leo, as expected from the spectral distribution of the stellar energy (see Fig. 1). O<sub>3</sub> most strongly absorbs at wavelengths below 0.5 μm where AD Leo does not emit much radiation, compared to the Sun.

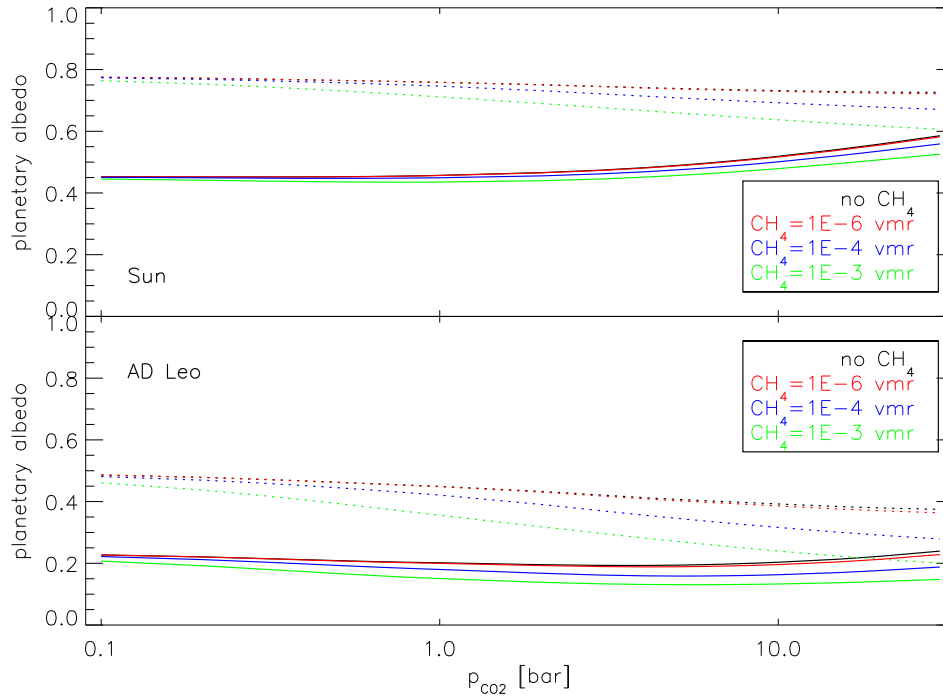


Figure 7: Planetary albedo as a function of  $\text{CO}_2$  pressure for snow and ice surface albedos. Influence of  $\text{CH}_4$  content. Plain lines for ice surface albedo, dotted lines for snow surface albedo.

## 4 Discussion of additional aspects

### 4.1 The effect of clouds

The main effect of clouds, such as in particular  $\text{H}_2\text{O}$  droplet and ice as well as  $\text{CO}_2$  ice clouds, in the visible and NIR is the scattering of incident stellar radiation. Due to their high and continuous opacities they can easily dominate the planetary albedo in this wavelength region.

Additionally, clouds can also limit the impact of the scattering by molecules and the surface on the planetary albedo. Shortwave radiation which is scattered

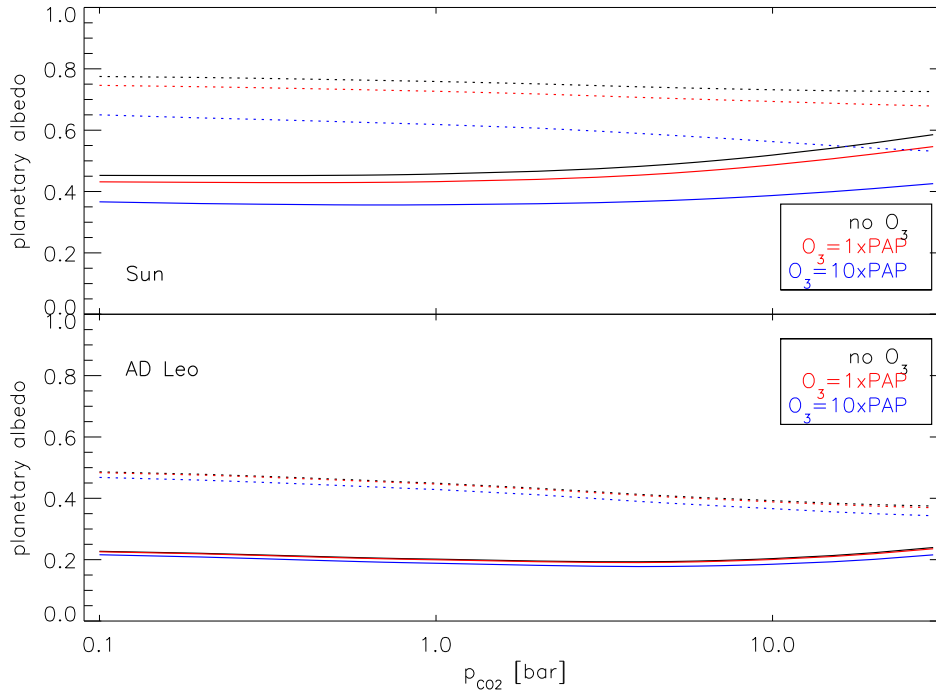


Figure 8: Planetary albedo as a function of CO<sub>2</sub> pressure for snow and ice surface albedos. Influence of O<sub>3</sub> content. Plain lines for ice surface albedo, dotted lines for snow surface albedo.

upwards by gas molecules or the surface can in turn be scattered down again by the cloud. Thus, the amount of downwelling short-wave radiation in the lower atmosphere can be higher if a cloud is present compared to the cloud-free cases presented in this study.

The exact impact on the incident stellar radiation is a direct function of the cloud's particle sizes. Particles with sizes near  $0.1 \mu\text{m}$  will have a Rayleigh scattering-like effect, i.e. they will contribute to the ice-albedo feedback in the same way as the scattering by gas molecules presented in this study. On the other hand, the optical properties of particles with sizes larger than a few  $\mu\text{m}$  are essentially flat

in the visible and NIR (e.g., Kitzmann et al. 2010). Compared to the cloud-free cases, this would lead to a constant offset in the planetary albedo which is almost independent from the incident stellar radiation (see e.g., Kitzmann et al. 2011 for H<sub>2</sub>O clouds and Kitzmann et al. 2013 for CO<sub>2</sub> clouds).

However, the presence of CO<sub>2</sub>, H<sub>2</sub>O, CH<sub>4</sub> and O<sub>3</sub> might inhibit cloud formation because of the warming of atmospheric layers by absorption of stellar radiation. Detailed atmospheric modeling is warranted to assess the possibility of cloud formation in the middle and upper atmosphere in future.

## 4.2 Land-ocean distribution

On Earth, the mean surface albedo is  $A_S=0.13$  (Rossow and Schiffer 1999), with the oceans ( $A_{\text{ocean}}=0.05$ ) being less reflective than the continents. The Martian surface albedo is much higher than this ( $A_{\text{mars}}=0.21$ , Kieffer et al. 1977). Also, different types of land (deserts, bare rock, forests, etc.) have different spectral surface albedos. Land plants have emerged not earlier than about 600 million years ago on Earth (e.g., Kasting and Howard 2006), which demonstrates that profound changes of a planets surface albedo might happen during its evolution. Therefore, it is expected that the land-ocean ratio and the distribution of continents might have a large influence on the overall surface albedo, and by extension, on the sensitivity of the planet to the ice-albedo feedback.

Since this land-ocean ratio and the continental distribution might also change during the planetary evolution (e.g., Pesonen et al. 2012), the strength of the ice-albedo effect might also change quite a lot over the course of the planetary evolution. An investigation with 2D or 3D atmosphere models would be necessary to

assess the strength of these effects.

### 4.3 Albedo measurements

Surface and atmospheric properties of terrestrial exoplanets such as continents, oceans or ice, snow, and cloud coverage induce photometric variability in the visible-near IR light curves and affect measured secondary eclipse albedos. Recent studies have suggested that it might be possible to infer such properties from spectro-photometric observations (e.g., Oakley and Cash 2009, Fujii et al. 2010, Livengood et al. 2011, Cowan et al. 2011). Albedo measurements might be indicative of snowball planets (e.g., Cowan et al. 2011). Such observations are easiest for transiting planets and could be performed near secondary eclipse. For hot giant planets, this has already been done (e.g., Snellen et al. 2009, Borucki et al. 2009, Parviainen et al. 2013).

Even if they were feasible for terrestrial, potentially habitable planets, it is questionable whether broadband photometric measurements of the reflected light could be useful to constrain the surface albedo and atmospheric characteristics. The contrast  $C_R$  between star and planet in reflected light close to secondary eclipse depends on planetary radius  $R_P$ , planetary albedo  $A_P$  and orbital distance  $d$ :

$$C_R = A_P \cdot f_R = A_P \cdot \left(\frac{R_P}{d}\right)^2 \quad (3)$$

For an Earth around the Sun ( $d=1$  AU), this translates into  $C_R \sim A_P \cdot 1.8 \times 10^{-9}$  (e.g., Kitzmann et al. 2011). If the planetary radius is known, the only uncertainty is on the deduced planetary albedo. Assuming a photometric precision of about

$2 \times 10^{-10}$  (i.e.,  $0.1 \times f_R$  in Eq. 3, Oakley and Cash 2009), the  $2\sigma$  uncertainty for the obtained planetary albedo  $A_p$  translates roughly to  $\pm 0.2$ .

As shown above in Sect. 3, albedo differences for the various scenarios are generally of this order of magnitude. This implies that albedo characterization is very difficult for planets orbiting around M stars. Distinguishing between low surface albedos and completely ice-covered planets is unlikely, even if the high albedo due to snow coverage could be excluded reasonably well. Furthermore, it is very difficult to infer the atmospheric properties (i.e., surface pressure, amount of radiative trace gases). For planets orbiting around Sun-like stars, it may be possible to distinguish between ice-free and ice-covered planets at low  $\text{CO}_2$  pressures. If a high albedo would be measured, however, the albedo solution is no longer unique, i.e. it might be an ice-covered planet at low or high atmospheric pressure or even an ice-free planet with a dense  $\text{CO}_2$  atmosphere or clouds.

Therefore, the characterization of the atmosphere and surface is not likely to be possible with secondary eclipse observations. To break degeneracies, additional observations are needed. Especially transmission spectroscopy during primary transit could be used to put constraints on atmospheric scale height and surface pressure (e.g., von Paris et al. 2011, Benneke and Seager 2012), thus helping to interpret measured planetary albedos. These observations would, however, require large telescope facilities to reach sufficient S/N ratios (e.g., Hedelt et al. 2013)

## 5 Summary and Conclusions

We have presented detailed calculations of the planetary albedo of terrestrial planets as a function of stellar type and atmospheric composition. Key atmospheric

properties such as CO<sub>2</sub> partial pressure and the abundance of radiative trace gases such as H<sub>2</sub>O, CH<sub>4</sub>, and O<sub>3</sub> were varied. Furthermore, we considered different types of surface albedo (wavelength-dependent ice or snow albedo, wavelength-independent constant albedo). Based on the planetary albedo, we investigated whether the ice-albedo feedback depends strongly on stellar type and atmospheric composition.

First, our calculations confirm the results of Joshi and Haberle (2012), i.e. that for ice- and snow-covered surfaces, the planetary albedos for planets orbiting M stars are much lower than for planets orbiting Sun-like stars (about a factor of two). This indeed leads to a strong reduction of the ice-albedo effect for planets around M stars.

Second, our results imply that for dense CO<sub>2</sub> atmospheres, the difference of planetary albedo between ice and ice-free ( $A_S=0.1$ ) cases is strongly reduced (from 0.35 to 0.05 for planets orbiting the Sun). For planets around M stars, the ice-albedo feedback is almost entirely masked at high CO<sub>2</sub> pressures (albedo change less than 0.04).

Third, we have shown that the effect of atmospheric composition may be very important when calculating the strength of the ice-albedo effect. Even radiative trace species such as H<sub>2</sub>O, CH<sub>4</sub>, or O<sub>3</sub> could alter sensitively the planetary albedo. This in turn influences the radiative forcing associated with an ice or snow surface albedo, hence could strongly suppress the ice-albedo feedback. The presence of small amounts of H<sub>2</sub>O and CH<sub>4</sub> effectively weakens the ice-albedo effect by several percent in planetary albedo for both stellar types considered. In addition, for planets around Sun-like stars, significant amounts of O<sub>3</sub> could also lead to a **very strong reduction** of the ice-albedo feedback at high CO<sub>2</sub> pressures.



## Acknowledgements

P. v. Paris and F. Selsis acknowledge support from the European Research Council (Starting Grant 209622: E<sub>3</sub>ARTHs). This research has been partly supported by the Helmholtz Association through the research alliance "Planetary Evolution and Life". Valuable discussions with P. Hedelt and J.L. Grenfell are gratefully acknowledged. Helpful, constructive comments by D. Abbot and an anonymous reviewer are also acknowledged.

## References

- D. S. Abbot, N. B. Cowan, and F. J. Ciesla. Indication of Insensitivity of Planetary Weathering Behavior and Habitable Zone to Surface Land Fraction. *Astrophys. J.*, 756:178, September 2012. doi: 10.1088/0004-637X/756/2/178.
- C.W. Allen. *Astrophysical Quantities*. The Athlone Press, University of London, 1973.
- B. Benneke and S. Seager. Atmospheric Retrieval for Super-Earths: Uniquely Constraining the Atmospheric Composition with Transmission Spectroscopy. *Astrophys. J.*, 753:100, July 2012. doi: 10.1088/0004-637X/753/2/100.
- W. J. Borucki, D. Koch, J. Jenkins, D. Sasselov, R. Gilliland, N. Batalha, D. W. Latham, D. Caldwell, G. Basri, T. Brown, J. Christensen-Dalsgaard, W. D. Cochran, E. DeVore, E. Dunham, A. K. Dupree, T. Gautier, J. Geary, A. Gould, S. Howell, H. Kjeldsen, J. Lissauer, G. Marcy, S. Meibom, D. Morrison, and

- J. Tarter. Kepler's Optical Phase Curve of the Exoplanet HAT-P-7b. *Science*, 325:709, August 2009. doi: 10.1126/science.1178312.
- R. E. Brandt, S. G. Warren, A. P. Worby, and T. C. Grenfell. Surface Albedo of the Antarctic Sea Ice Zone. *Journal of Climate*, 18:3606–3622, September 2005. doi: 10.1175/JCLI3489.1.
- N. B. Cowan, T. Robinson, T. A. Livengood, D. Deming, E. Agol, M. F. A'Hearn, D. Charbonneau, C. M. Lisse, V. S. Meadows, S. Seager, A. L. Shields, and D. D. Wellnitz. Rotational Variability of Earth's Polar Regions: Implications for Detecting Snowball Planets. *Astrophys. J.*, 731:76, April 2011. doi: 10.1088/0004-637X/731/1/76.
- S. Domagal-Goldman and V. Meadows. Abiotic buildup of ozone. *ASP Conference Series*, 430:152, 2010.
- Y. Fujii, H. Kawahara, Y. Suto, A. Taruya, S. Fukuda, T. Nakajima, and E. L. Turner. Colors of a Second Earth: Estimating the Fractional Areas of Ocean, Land, and Vegetation of Earth-like Exoplanets. *Astrophys. J.*, 715:866–880, June 2010. doi: 10.1088/0004-637X/715/2/866.
- C. Goldblatt, T. M. Lenton, and A. J. Watson. Bistability of atmospheric oxygen and the Great Oxidation. *Nature*, 443:683–686, October 2006. doi: 10.1038/nature05169.
- J. L. Grenfell, J.-M. Grießmeier, B. Patzer, H. Rauer, A. Segura, A. Stadelmann, B. Stracke, R. Titz, and P. Von Paris. Biomarker Response to Galactic Cosmic Ray-Induced NO<sub>x</sub> And The Methane Greenhouse Effect in The Atmosphere of

- An Earth-Like Planet Orbiting An M Dwarf Star. *Astrobiology*, 7:208–221, February 2007. doi: 10.1089/ast.2006.0129.
- J. L. Grenfell, S. Gebauer, P. von Paris, M. Godolt, P. Hedelt, A. B. C. Patzer, B. Stracke, and H. Rauer. Sensitivity of biomarkers to changes in chemical emissions in the Earth’s Proterozoic atmosphere. *Icarus*, 211:81–88, January 2011. doi: 10.1016/j.icarus.2010.09.015.
- P. Hedelt, P. von Paris, M. Godolt, S. Gebauer, J. L. Grenfell, H. Rauer, F. Schreier, F. Selsis, and T. Trautmann. Spectral features of Earth-like planets and their detectability at different orbital distances around F, G, and K-type stars. *Astron. Astrophys.*, 553:A9, May 2013. doi: 10.1051/0004-6361/201117723.
- P. F. Hoffman, A. J. Kaufman, G. P. Halverson, and D. P. Schrag. A Neoproterozoic Snowball Earth. *Science*, 281:1342, August 1998. doi: 10.1126/science.281.5381.1342.
- S. R. Hudson, S. G. Warren, R. E. Brandt, T. C. Grenfell, and D. Six. Spectral bidirectional reflectance of Antarctic snow: Measurements and parameterization. *Journal of Geophysical Research (Atmospheres)*, 111:D18106, September 2006. doi: 10.1029/2006JD007290.
- W. T. Hyde, T. J. Crowley, S. K. Baum, and W. R. Peltier. Neoproterozoic ‘snowball Earth’ simulations with a coupled climate/ice-sheet model. *Nature*, 405: 425–429, May 2000.
- M. M. Joshi and R. M. Haberle. Suppression of the Water Ice and Snow Albedo Feedback on Planets Orbiting Red Dwarf Stars and the Subsequent Widening

- of the Habitable Zone. *Astrobiology*, 12:3–8, January 2012. doi: 10.1089/ast.2011.0668.
- E. Karkoschka. Spectrophotometry of the jovian planets and Titan at 300- to 1000-nm wavelength: The methane spectrum. *Icarus*, 111:174–192, September 1994. doi: 10.1006/icar.1994.1139.
- J. F. Kasting and M. T. Howard. Atmospheric composition and climate on the early Earth. *Phil. Trans. R. Soc. B*, 361:1733–1742, 2006.
- J. F. Kasting and S. Ono. Palaeoclimates: the first two billion years. *Phil. Trans. R. Soc. B*, 361:917–929, 2006.
- J. F. Kasting, D. P. Whitmire, and R. T. Reynolds. Habitable Zones around Main Sequence Stars. *Icarus*, 101:108–128, January 1993. doi: 10.1006/icar.1993.1010.
- H. H. Kieffer, T. Z. Martin, A. R. Peterfreund, B. M. Jakosky, E. D. Miner, and F. D. Palluconi. Thermal and albedo mapping of Mars during the Viking primary mission. *J. Geophys. Res.*, 82:4249–4291, September 1977. doi: 10.1029/JS082i028p04249.
- J. Kirschvink. Late Proterozoic low-latitude global glaciation: The snowball Earth . In *The Proterozoic Biosphere: A Multidisciplinary Study*, pages 51–52, 1992.
- D. Kitzmann, A. B. C. Patzer, P. von Paris, M. Godolt, B. Stracke, S. Gebauer, J. L. Grenfell, and H. Rauer. Clouds in the atmospheres of extrasolar planets. I. Climatic effects of multi-layered clouds for Earth-like planets and implications for habitable zones. *Astron. Astrophys.*, 511:A66, March 2010.

- D. Kitzmann, A. B. C. Patzer, P. von Paris, M. Godolt, and H. Rauer. Clouds in the atmospheres of extrasolar planets. III. Impact of low and high-level clouds on the reflection spectra of Earth-like planets. *Astron. Astrophys.*, 534:A63, October 2011. doi: 10.1051/0004-6361/201117375.
- D. Kitzmann, A. B. C. Patzer, and H. Rauer. Clouds in the atmospheres of extrasolar planets. IV. On the scattering greenhouse effect of CO<sub>2</sub> ice particles: Numerical radiative transfer studies. *accepted in Astron. Astrophys.*, June 2013.
- S. K. Leggett, F. Allard, G. Berriman, C. C. Dahn, and P. H. Hauschildt. Infrared Spectra of Low-Mass Stars: Toward a Temperature Scale for Red Dwarfs. *Astrophys. J. Suppl.*, 104:117–143, May 1996. doi: 10.1086/192295.
- T. A. Livengood, L. D. Deming, M. F. A’Hearn, D. Charbonneau, T. Hewagama, C. M. Lisse, L. A. McFadden, V. S. Meadows, T. D. Robinson, S. Seager, and D. D. Wellnitz. Properties of an Earth-Like Planet Orbiting a Sun-Like Star: Earth Observed by the EPOXI Mission. *Astrobiology*, 11:907–930, November 2011. doi: 10.1089/ast.2011.0614.
- C. P. McKay, J. B. Pollack, and R. Courtin. The thermal structure of Titan’s atmosphere. *Icarus*, 80:23–53, July 1989. doi: 10.1016/0019-1035(89)90160-7.
- M. A. Mischna, J. F. Kasting, A. Pavlov, and R. Freedman. Influence of carbon dioxide clouds on early martian climate. *Icarus*, 145:546–554, June 2000. doi: 10.1006/icar.2000.6380.
- P. H. H. Oakley and W. Cash. Construction of an Earth Model: Analysis of Exoplanet Light Curves and Mapping the Next Earth with the New Worlds Ob-

- server. *Astrophys. J.*, 700:1428–1439, August 2009. doi: 10.1088/0004-637X/700/2/1428.
- H. Parviainen, H. J. Deeg, and J. A. Belmonte. Secondary eclipses in the CoRoT light curves. A homogeneous search based on Bayesian model selection. *Astron. Astrophys.*, 550:A67, February 2013. doi: 10.1051/0004-6361/201220081.
- A. A. Pavlov, J. F. Kasting, L. L. Brown, K. A. Rages, and R. Freedman. Greenhouse warming by CH<sub>4</sub> in the atmosphere of early Earth. *J. Geophys. Res.*, 105: 11981–11990, May 2000. doi: 10.1029/1999JE001134.
- A. A. Pavlov, M. T. Hurtgen, J. F. Kasting, and M. A. Arthur. Methane-rich Proterozoic atmosphere? *Geology*, 31:87–90, January 2003. doi: 10.1130.
- L. Pesonen, S. Mertanen, and T. Veikkolainen. Paleo-Mesoproterozoic Supercontinents A Paleomagnetic View. *Geophysica*, 48:5–47, January 2012.
- W. B. Rossow and R. A. Schiffer. Advances in Understanding Clouds from ISCCP. *Bull. Americ. Meteor. Soc.*, 80:2261–2288, November 1999. doi: 10.1175/1520-0477(1999)080<2261:AIUCFI>2.0.CO;2.
- A. Segura, J. F. Kasting, V. Meadows, M. Cohen, J. Scalo, D. Crisp, R. A. H. Butler, and G. Tinetti. Biosignatures from Earth-Like Planets Around M Dwarfs. *Astrobiology*, 5:706–725, December 2005. doi: 10.1089/ast.2005.5.706.
- A. Segura, V. S. Meadows, J. F. Kasting, D. Crisp, and M. Cohen. Abiotic formation of O<sub>2</sub> and O<sub>3</sub> in high-CO<sub>2</sub> terrestrial atmospheres. *Astron. Astrophys.*, 472: 665–679, 2007.

- F. Selsis, D. Despois, and J.-P. Parisot. Signature of life on exoplanets: Can Darwin produce false positive detections? *Astron. Astrophys.*, 388:985–1003, June 2002. doi: 10.1051/0004-6361:20020527.
- F. Selsis, J. F. Kasting, B. Levrard, J. Paillet, I. Ribas, and X. Delfosse. Habitable planets around the star Gliese 581? *Astron. Astrophys.*, 476:1373–1387, December 2007. doi: 10.1051/0004-6361:20078091.
- A. L. Shields, V. S. Meadows, C. M. Bitz, R. T. Pierrehumbert, M. M. Joshi, and T. D. Robinson. The Effect of Host Star Spectral Energy Distribution and Ice-Albedo Feedback on the Climate of Extrasolar Planets. *accepted in Astrobiology*, May 2013.
- I. A. G. Snellen, E. J. W. de Mooij, and S. Albrecht. The changing phases of extrasolar planet CoRoT-1b. *Nature*, 459:543–545, May 2009. doi: 10.1038/nature08045.
- L. Tarasov and W. R. Peltier. Terminating the 100 kyr ice age cycle. *J. Geophys. Res.*, 102:21665–21694, 1997. doi: 10.1029/97JD01766.
- O. B. Toon, C. P. McKay, T. P. Ackerman, and K. Santhanam. Rapid calculation of radiative heating rates and photodissociation rates in inhomogeneous multiple scattering atmospheres. *J. Geophys. Res.*, 94:16287–16301, 1989.
- I. M. Vardavas and J. H. Carver. Solar and terrestrial parameterizations for radiative-convective models. *Planet. Space Science*, 32:1307–1325, October 1984. doi: 10.1016/0032-0633(84)90074-6.
- P. von Paris, S. Gebauer, M. Godolt, J. L. Grenfell, P. Hedelt, D. Kitzmann,

- A. B. C. Patzer, H. Rauer, and B. Stracke. The extrasolar planet GL 581 d: A potentially habitable planet? *Astron. Astrophys.*, 522:A23, November 2010. doi: 10.1051/0004-6361/201015329.
- P. von Paris, J. Cabrera, M. Godolt, J. L. Grenfell, P. Hedelt, H. Rauer, F. Schreier, and B. Stracke. Spectroscopic characterization of the atmospheres of potentially habitable planets: GL 581 d as a model case study. *Astron. Astrophys.*, 534:A26, October 2011. doi: 10.1051/0004-6361/201117091.
- J. C. G. Walker, P. B. Hays, and J. F. Kasting. A negative feedback mechanism for the long-term stabilization of the earth's surface temperature. *J. Geophys. Res.*, 86:9776–9782, October 1981. doi: 10.1029/JC086iC10p09776.
- W. J. Wiscombe and J. Evans. Exponential-sum fitting of radiative transmission functions. *J. Computational Physics*, 24:416–444, 1977.
- R. D. Wordsworth, F. Forget, F. Selsis, E. Millour, B. Charnay, and J.-B. Madeleine. Gliese 581d is the First Discovered Terrestrial-mass Exoplanet in the Habitable Zone. *Astrophys. J. Letters*, 733:L48, June 2011. doi: 10.1088/2041-8205/733/2/L48.